

RESEARCH ARTICLE

Multilevel Pulse Position Modulation With Level Trimming for Electromagnetic Nanocommunications in the Terahertz Band

PANKAJ SINGH^{ID}, (Member, IEEE), AND SUNG-YOON JUNG^{ID}, (Member, IEEE)

Department of Electronic Engineering, Yeungnam University, Gyeongsan, Gyeongsangbuk 38541, South Korea

Corresponding author: Sung-Yoon Jung (syjung@ynu.ac.kr)

This work was supported by the National Research Foundation of Korea (NRF) Grants funded by the Korean Government under Grant NRF-2022R1G1A1004799 and Grant NRF-2018R1A2B6002204.

ABSTRACT Nanomachines are submicrometer-scale devices led by nanotechnology that can perform simple sensing, local actuation, limited data processing, storage, and communication tasks in the terahertz (THz) band, that is, from 0.1-10 THz. Electromagnetic nanocommunication among nanomachines results in a nanonetwork which could breakthrough promising applications in multiple domains such as software-defined metamaterials, in-body communication, and on-chip communication. This study adopts a modulation scheme for nanomachine communication based on *multilevel* pulse position modulation (ML-PPM). The multilevel scheme uses several orthogonal codes and is combined with PPM to generate the final transmit signal consisting of several multilevels. In this paper, we propose a more advanced scheme called *level trimming* to further boost the data rates of the ML-PPM scheme. Employing level-trimming, we transmit a fewer number of levels than required in ML-PPM, which will result in an spectral efficiency gain at the nanoreceiver. The simulation results reveal that the link capacity of the proposed scheme can be increased more than twofold using the level-trimming approach while the error rate performance remains better than the conventional ML-PPM. For instance, ML-PPM with level trimming achieves a data rate of approximately 4.5 terabits per second (Tbps) when trimming the levels from seven to one compared to ML-PPM that achieves around 1 Tbps under the same network conditions. At the same time, a 2 dB gain in BER performance is achieved with level trimming. Moreover, the computational complexity of nanotransceivers is reduced with the transmission of fewer levels. Furthermore, although level-trimming causes artificial errors, it improves the decoding performance by reducing the number of levels. We believe that the potential impact of this study will open doors for further investigations on various possible modulation formats for THz nanocommunication.

INDEX TERMS Level trimming, multilevel, nanocommunication, pulse position modulation, terahertz band.

I. INTRODUCTION

Nanomachines, which are typically nano to micro-sized devices that can perform simple tasks such as sensing, local actuation, storage, and limited computation at the nanolevel,

The associate editor coordinating the review of this manuscript and approving it for publication was Saroj Tripathi^{ID}.

are under investigation as a breakthrough in nanotechnology [1], [2]. Communication among nanomachines, that is, nanocommunication [3], [4], [5], increases the range of operation and capability of a nanomachine manifold to accomplish complex tasks. The resulting nanonetwork [2], [5], [6], [7], [8] can enable new advanced applications of nanotechnology in the fields of biomedicine [9], [10],

environment [5], [8], and military [7], [8], [11]. One of the forefront applications of nanonetworks lies in the medical field for in-body communications. For example, mobile medical nanodevices can access regions of the human body, such as blood vessels and the brain, and monitor the levels of nutrients in real time. In addition, nanomachines can aid in the early diagnosis and treatment of malicious agents, such as viruses and cancer cells. This can enable pioneering applications such as immune system support, bio-hybrid implants, targeted drug delivery systems, and real-time health monitoring [3]. In case of the environment, chemical nanosensors can be used for crop monitoring, bio-degradation assistance, and air pollution control [4]. Similarly, chemical and biological nanosensors can be used to detect harmful chemicals and biological weapons in a distributed manner [2]. A wireless nanosensor network can converge information on the molecular composition of air at a specific location to a macro device in a very short time. In addition, nanocommunication forms an essential part of future wireless communication, which includes 6G and beyond 6G networks [12], [13] and the Internet of nano things (IoNT) [14], [15], [16]. Using IoNT, a nanotransceiver can be embedded in every object, thereby allowing it to be permanently connected to the internet.

Several nanocommunication paradigms have been proposed in the literature, including electromagnetic (EM), molecular, and acoustic communications. Among these, EM nanocommunication is the foremost research area, which can be realized in the terahertz (THz) band, that is, from 0.1-10 THz [3], [11], [17], [18], [19], [20]. This can be attributed to the discovery of novel nanomaterials, such as graphene and carbon nanotubes, which exhibit promising electrical and optical properties and support the transmission of surface plasmon polariton (SPP) waves with THz frequencies [21], [22], [23]. In addition, the THz band has been extensively explored from different aspects over the last decade for future wireless communication [11], [19], [24], [25]. Moreover, in 2019, the U.S. Federal Communications Commission licensed the use of THz frequency, specifically, from 95 GHz to 3 THz, to develop 6G technology in subTHz frequency bands. This license is called the spectrum horizon license [26]. Therefore, EM nanocommunication in the THz band is envisioned as a key technology for ubiquitous wireless communications beyond 5G. More importantly, the application domains of nanonetworks, including the Internet of multimedia nanothings [16] and bio-nano things [27], require ultrahigh-speed data rates in the terabits per second (Tbps) range, which could be accomplished using the THz nanocommunications [28].

Although nanocommunication has considerable potential, it suffers from certain fundamental challenges, as techniques to establish communication between nanomachines are yet to be developed. This can be attributed to several reasons. First, conventional communication techniques cannot be directly applied to the nanoscale domain. Nanodevices are extremely small-scale devices, and the properties of materials here differ significantly from those at the macroscale. In addition,

owing to the nanoscale dimensions, there exist size, memory, and signal generation, as well as signal processing, constraints on the nanomachines. For example, conventional high-frequency carrier-based communication cannot be used for nanoscale communication, predominantly owing to the ultra-small size and limited capabilities of nanodevices [22], [23]. Moreover, the generation and reception of ultrahigh-frequency carrier signals require power-hungry circuits and processors, which is not feasible at the nanolevel. Overall, the nanoscale dimension imposes stringent restrictions on size and power, which indicates the pressing need for simple and ultraefficient modulations. Moreover, state-of-the-art wireless technologies still cannot support Tbps links [11]. Therefore, carrier-less communication can be considered as an alternative [29]. In other words, pioneering research on nanonetworks discourages the use of methods that require significant signal processing and suggests pulse-based communication as a alternative to achieve Tbps data rates simultaneously [28], [30], [31]. In [28], the authors analyzed the THz channel and proposed the use of an ultrashort one-hundred femtosecond long pulse for transferring information bits. The scheme proposed in [30] depends on the emission of femtosecond-long Gaussian pulses by adopting on-off keying modulation. Conversely, the scheme proposed in [31] follows pulse position modulation (PPM) utilizing the same one-hundred-femtosecond-long Gaussian pulses.

Along the same lines, in our previous study, we developed a modulation scheme for THz band-based nanocommunication called *multilevel* pulse position modulation (ML-PPM) [32]. A multilevel scheme uses several orthogonal codes simultaneously and is combined with a PPM scheme to achieve not only variable and high data rates but also processing gain at the nanoreceiver end, thereby guaranteeing the benefits of PPM. This paper proposes an enhanced version of the conventional ML-PPM scheme. In particular, we employ a new technique called *level trimming* to the conventional ML-PPM. In the conventional ML-PPM, the probability that multilevel signals have larger values is small and smaller values is large. In other words, the multilevel signal follow a binomial distribution. In this study, using the level-trimming approach, we trim our multilevel signal to transmit only the levels with higher occurrence probabilities and eliminate levels with lower occurrence probabilities. That is, we prohibit the transmission of levels that occur with lower probabilities. This results in two effects: First, this will increase the data rate with additional performance enhancement, and second, this can significantly reduce computational complexity at the nanoreceiver. Moreover, we analyze how transmitting fewer levels with higher probabilities boosts the data rate of the ML-PPM. The primary contributions of this study are as follows.

- 1) The proposed scheme with a level-trimming approach increases the data rate of the THz nanocommunication system by over two times with a lower number of levels, thereby achieving spectral gain in the THz band and spectral-efficient modulation.

- 2) The bit error rate (BER) performance of the proposed scheme is compared with that of the conventional ML-PPM scheme, and the results reveal that the proposed scheme performs better.
- 3) The computational complexity of transceivers is reduced comparatively by the transmission of fewer levels.

The remainder of the paper is organized as follows. Section II provides an overview of the conventional ML-PPM scheme. In Section III, we introduce the level-trimming scheme in ML-PPM and discuss how level trimming achieves spectral efficiency along with a signal model. Section IV describes the THz propagation environment in which the simulations were carried out. In Section V, we model the nanoreceiver along with THz noise and show how level trimming reduces the nanoreceiver complexity manifolds without affecting the data rates. Through simulations, in Section VI, we confirm that the proposed ML-PPM with level trimming presents an improved BER curve and a significantly greater achievable data rate compared to the conventional ML-PPM under the same nanocommunication channel environment. Finally, Section VII concludes the paper.

II. BACKGROUND OF MULTILEVEL PULSE POSITION MODULATION

First, we describe the conventional ML-PPM scheme. Fig. 1 illustrates a block diagram of the proposed ML-PPM with a level-trimming scheme; note that the figure essentially illustrates the conventional ML-PPM scheme if the level-trimming block is excluded. Each data block comprises L binary phase-shift keying modulated data $\mathbf{b} = [b_1, \dots, b_L]^T$, which are then encoded by L binary orthogonal codes of length N_p to obtain a multilevel signal vector as follows:

$$\mathbf{d} = \mathbf{S} \cdot \mathbf{b} = [d_1, \dots, d_{N_p}]^T, \quad (1)$$

where

$$\mathbf{S} = [s_1, \dots, s_L] \quad (2)$$

is an $N_p \times L$ binary orthogonal code matrix, and $s_l = [s_{1,l}, \dots, s_{N_p,l}]^T$, $s_{n,l} \in \{+1, -1\}$ denotes the l th orthogonal code. Then, each element of \mathbf{d} has $L + 1$ symmetric possible multilevel values, that is, $d_n = \{-L, -L + 2, \dots, L - 2, L\}$. In addition, $L \leq N_p - 1$. In other words,

$$N_p \geq 2^m, \quad (3)$$

where

$$m = \lceil \log_2(L) \rceil. \quad (4)$$

Subsequently, each element of \mathbf{d} is then pulse position modulated to generate a pulse position vector, given as

$$\mathbf{m} = [m_1, \dots, m_{N_p}]^T, \quad (5)$$

with

$$m_n = \frac{d_n + L}{2}, \quad (6)$$

where m_n denotes the delay in determining the pulse position. Note that we only require $L + 1$ positions to transmit L bits, which is the central idea of the ML-PPM scheme. For simplicity, we omit the multiple-access scheme [32] and assume a single user case. After passing through the THz pulse shaping filter, the transmitted THz signal in ML-PPM has the form

$$s(t) = \sum_{i=-\infty}^{\infty} \sum_{n=0}^{N_p-1} p(t - iT_s - nT_f - m_n\delta), \quad (7)$$

where δ denotes the pulse spacing between two consecutive emission time slots, and $p(t)$ represents a one-hundred-femtosecond long Gaussian pulse with a duration T_p and energy E_p . The transmitted signal, which contains L data, occupies a total of N_p frames with a duration T_f and requires a time duration $T_s = N_p T_f$, where $T_f = (L + 1)\delta$. The basic THz pulse $p(t)$ is Gaussian in nature and is defined as

$$p(t) = \frac{\alpha}{\sqrt{2\pi}\sigma} e^{-(t-\mu)^2/2\sigma^2}, \quad (8)$$

where α is a constant, σ is the standard deviation, and μ is the pulse mean. The pulse energy E_p can be expressed as $E_p = \int_{-\infty}^{\infty} p^2(t) dt$. The width of the pulse is chosen to be ultrashort at just 100 fs, and the energy is considered on the order of attojoules ($1 \text{ aJ} = 10^{-18} \text{ J}$).

The reason for choosing a 100 fs-long pulse is supported by the recent developments in state-of-the-art THz band signal generators and detectors. First, from the hardware perspective, the application of a voltage between the source and drain of a high-electron-mobility transistor (HEMT) excites SPP waves. At room temperature, SPP waves are overdamped, which only generates broadband incoherent waveforms, that is, extremely short pulse-like radiation (one-hundred-femtosecond long) [30]. Additionally, the generated SPP wave can be radiated by graphene-based plasmonic nanoantennas [22]. During reception, the injection of SPP waves into the channel of the HEMT results in electrons being pushed from the source to the drain, thereby generating a voltage difference between them. Second, the major spectral components of these pulses are contained within the THz band [28]. Considering the THz propagation environment and support of SPP waves at THz frequencies by the HEMTs and graphene nanoantennas, the power spectral density (p.s.d.) of the transmitted pulse is centered around 1.6 THz with a 3 dB bandwidth between 0.7-2.5 THz. As we will describe in Section IV, frequency directly affects spreading losses in THz channels. Therefore, it is appropriate to work in the initial part of the THz band with a pulse whose p.s.d. is centered at approximately 1.6 THz. The Gaussian nature of the pulse is chosen based on the simplicity with which it can be realized [28]. From a hardware perspective, the time derivatives of the Gaussian pulse can be easily obtained by combining nanoscale delay lines [30]. Owing to the nanoantenna transfer function, the first time derivative of the Gaussian pulse is transmitted.

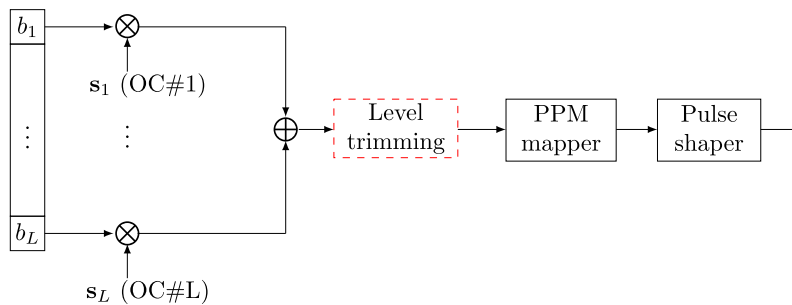


FIGURE 1. Block diagram of the proposed ML-PPM with level trimming.

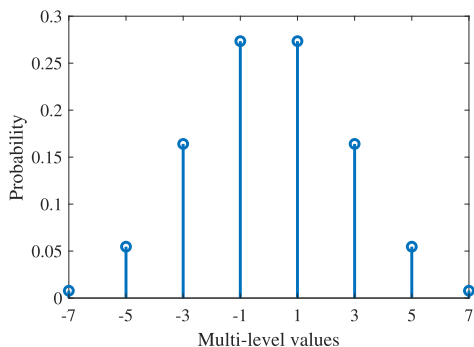


FIGURE 2. Binomial distribution of a typical ML-PPM signal with $L = 7$ and $N_p = 8$.

III. PROPOSED LEVEL TRIMMING SCHEME

Fig. 1 illustrates a block diagram of the proposed ML-PPM with level trimming. Further, we consider Fig. 1 with a level trimming block. As can be observed, we trim out multilevel values before mapping them to the pulse positions. Level trimming implies that we do not map all multilevels to the pulse position. We exclude some of the insignificant levels and map a short version of the multilevel vector to the pulse position. This can be achieved based on the following criteria. Orthogonal codes used to generate the multilevel signal, d_n , in (1) follow the tendency of the random binary code to exhibit equal probability with possible values $\{+1, -1\}$ when L is sufficiently large. Therefore, we can conclude that the probability $P\{d_n = l\}$ follows a binomial distribution [33]:

$$P\{d_n = l\} = \binom{L}{(l+L)/2} \left(\frac{1}{2}\right)^L, \quad (9)$$

where

$$\binom{p}{q} = \frac{p!}{q!(p-q)!}. \quad (10)$$

From the above equation, we can observe that the probability that the multilevel signal has a large value is small. For instance, the probability that a multilevel signal will have a value of 1 (or -1) is 0.2734. This can also be observed in Fig. 2. As values of L becomes large, the multilevels become smaller. In the conventional ML-PPM

(see Section II) [32], after generating the transmitted signal, as shown in (7), we transmit all the generated positions regardless of their different occurrence probabilities. Intuitively, we can observe that it is better to transmit the multilevels with large occurrence probabilities and eliminate the multilevels, which occurs with small probabilities. In other words, we are transmitting several multilevels with high probabilities in place of multilevels having low occurrence probabilities. This will definitely going to increase the data rate as the time duration of the final symbol is getting reduced (due to elimination of some levels). Furthermore, that time period is utilized in transmitting the next symbol, hence, improving the spectral efficiency. In addition, even though we do not transmit the multilevels having small occurrence probabilities, it will not degrade the performance much as these multilevel do not occur frequently. On the contrary, the BER performance improves compared to conventional ML-PPM as level trimming improves the decoding performance by reducing the number of levels. In addition, level trimming decreases the computation complexity at the nanoreceiver, which requires each level to process. Note that now, the nanoreceiver has to process a trimmed (reduced) vector size rather than a full transmit vector. Hence, the signal processing in the demodulation stage is significantly reduced.

Focusing on this phenomenon, we propose a simple and powerful method to enhance the data rates of the proposed scheme via level trimming. In level trimming, we trim the final ML-PPM signal to only transmit levels with higher occurrence probabilities and restrict the levels with lower probabilities of occurrence. In this a manner, we can maximize the spectral efficiency of the ML-PPM and increase the achievable data rate significantly. This can be attributed to the inter-relation between the three key parameters of the proposed scheme, that is, the occurrence probabilities of multilevels, trimming threshold, and the spectral efficiency. As presented in Fig. 2, the ML-PPM signal has a binomial distribution. First, if the number of multilevels (L) increases, the occurrence probabilities of tails on both sides of the distribution become significantly low. In such cases, we can increase the trimming threshold to trim more levels that occur with lower probabilities. Conversely, if the number of multilevels is low, we cannot increase the trimming threshold,

TABLE 1. PPM mapping rule as per (12).

d_n	m_n
$-L_{th}$	0
$-L_{th} + 2$	1
$-L_{th} + 4$	2
\vdots	\vdots
$L_{th} - 4$	$L_{th} - 2$
$L_{th} - 2$	$L_{th} - 1$
L_{th}	L_{th}

considering that all multilevels occur with similar probabilities. Second, if we increase the trimming threshold, the spectral efficiency will increase as more bits can be transmitted per hertz within a given bandwidth. Therefore, trimming threshold directly affects the spectral efficiency. Third, this significantly reduces the computational complexity at the nanoreceiver. The nanoreceiver must now process fewer slots to obtain the signal energy and estimate the transmitted bit. Therefore, we perform trimming of the multilevel signal that exceeds the trimming threshold.

A. SIGNALING FORMAT

If we let the limited maximum trimming threshold of the multilevel signal be $L_{th}(\leq L)$, the number of each multilevel values of d_n is eliminated to $L_{th} + 1$ with a range of $\{-L_{th}, -L_{th} + 2, \dots, L_{th} - 2, L_{th}\}$. Then, each element of a multilevel signal vector is converted into a pulse position vector as

$$\mathbf{m}^{th} = [m_1^{th}, \dots, m_{N_p}^{th}]^T, \tag{11}$$

where

$$m_n^{th} = \frac{d_n + L_{th}}{2}. \tag{12}$$

Therefore, from (7), the transmitted signal for the ML-PPM with a level-trimming scheme can be expressed as

$$s^{th}(t) = \sum_{i=-\infty}^{\infty} \sum_{n=0}^{N_p-1} p(t - iT_s - nT_f - m_n^{th}\delta). \tag{13}$$

For an easier understanding, we present the PPM mapping rule in Table 1 for all possible multilevels.

As mentioned above, the level-trimming scheme maximizes spectral efficiency. This can easily be observed via a simple example. Considering $N_p = 4$ and $L = 3$, the symbol duration T_s becomes $T_s = N_p(L + 1)\delta = 4 \cdot 4 \cdot \delta = 16\delta$. Using the level-trimming scheme, we set $L_{th} = 1$. Therefore, $T_s = 4 \cdot 2 \cdot \delta = 8\delta$. That is, the symbol duration can be reduced by half by employing a level-trimming scheme. As a result, the data rate of the ML-PPM with a level-trimming scheme is $(L + 1)/(L_{th} + 1)$ times higher than that of the conventional ML-PPM scheme. However, the level-trimming scheme inevitably suffers from artificial errors. Nevertheless, transmitting only a lower number of levels having higher

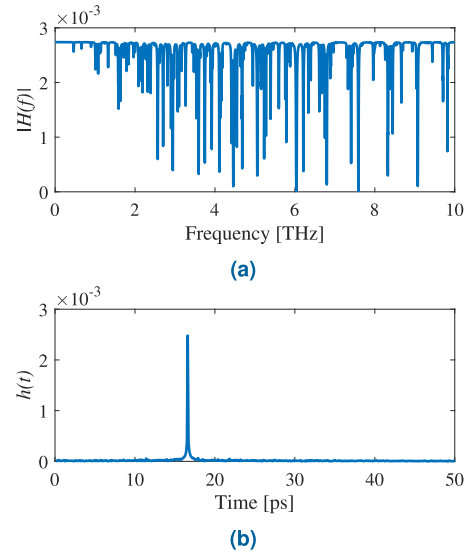


FIGURE 3. Terahertz channel with 10% water vapor concentration for a distance of 5 mm. (a) Channel frequency response showing frequency selectivity behavior and (b) channel impulse response showing the attenuation and time delay in reception.

occurrence probabilities results in better BER performance. We will discuss this in the simulation results section.

IV. PROPAGATION IN THE TERAHERTZ CHANNEL

Unlike a conventional macroscale wireless network, in a nanonetwork, the nanomachines are separated only by a few nano to micrometers. Fortunately, in this distance range, the THz band provides extremely large bandwidth, that is, an almost 10 THz wide communication window [28]. However, simultaneously, the THz band is highly affected by the water vapor concentration in the transmission medium owing to the fact that the presence of water vapor molecules in the medium results in the rise of molecular absorption loss. Therefore, as the medium becomes humid, the communication range decreases significantly.

A path loss model for the entire THz band, i.e., from 0.1-10 THz, was presented in the pioneering work conducted in [28]. Therefore, we can conclude that the THz channel is highly distance dependent and frequency selective. The total path loss A for a traveling EM wave in THz channel can be described by combining the spreading loss A_{spr} and molecular absorption loss A_{abs} as [28]

$$A(f, d) = A_{spr}(f, d)A_{abs}(f, d), \tag{14}$$

where f is the wave frequency, and d is the distance between nanomachines. The spreading loss and molecular absorption loss can be further expressed as

$$A_{spr}(f, d) = \left(\frac{4\pi fd}{c}\right)^2 \tag{15}$$

and

$$A_{abs}(f, d) = \frac{1}{e^{-k(f)d}}, \tag{16}$$

where c is the speed of light, and $k(f)$ is the frequency-dependent medium absorption coefficient [28]. The path losses are related to the THz channel frequency response, $H(f, d)$, as [30]

$$\begin{aligned} H(f, d) &= \left(\frac{1}{\sqrt{A(f, d)}} \right) e^{-j2\pi fd/c} \\ &= \left(\frac{1}{\sqrt{4\pi d}} \right) e^{-k(f)d/2} e^{-j(2\pi fd/c)}. \end{aligned} \quad (17)$$

Following this, the THz channel impulse response can be easily computed by taking the inverse Fourier transform of the above equation as

$$h(t, d) = \mathcal{F}^{-1}[H(f, d)]. \quad (18)$$

Note that the impulse response doesn't have a closed-form and is evaluated numerically.

Fig. 3 presents one of the THz channel realizations. The THz channel was concentrated with 10% water vapor, and the pulse propagation distance was fixed at 5 mm. In the channel frequency response, that is, Fig. 3a, the frequency selectivity of the channel could be observed. That is, the attenuation varied significantly for different frequencies across the band. Furthermore, the THz channel time response, that is, Fig. 3b, revealed the attenuation of a propagating pulse, as well as the time of arrival of the pulse at the nanoreceiver. Additionally, several small ripples can be observed in the impulse response owing to the impact of molecular absorption loss in the channel, as described above. However, note that the impact of molecular absorption is quite negligible at the range of nanocommunication distances; this is because in the current scenario, we considered the water vapor concentration in a normal environment. However, as the water vapor concentration increases, the formation of ripples becomes significant, thereby leading to further degradation of the transmitted signal.

V. NANORECEIVER SIGNAL PROCESSING

The transmitted pulse was received by the nanoreceiver after passing through the THz channel. The received signal can be expressed as

$$r(t) = s(t) * h(t) + n_{awg}(t) + n_{bck}(t), \quad (19)$$

where $h(t)$ is the impulse response of the THz channel, $n_{awg}(t)$ is additive white Gaussian noise (AWGN), and $n_{bck}(t)$ is the background noise of the transmission medium. Similar to conventional communications, two primary sources of noise are noted in THz communications [34]: 1) electronic thermal noise arising at the nanoreceiver, and 2) molecular absorption noise induced by water vapor molecules [35]. For the thermal noise, the corresponding histogram of the measured noise follows a Gaussian distribution, according to the noise behavior at lower frequencies. As far as the absorption noise is concerned, it consists of background noise that uses sky noise as a basis [35], [36]. In our simulation

setup, the nanocommunication distance between the nanotransmitter and nanoreceiver was set to 0.5 mm for which we will compute the background noise next.

The atmospheric noise is caused by the temperature of the absorbing medium, making the medium an effective black body radiator [35]. This atmospheric noise is therefore known as a background noise and can be derived from the Planck's law. This is because Planck's law gives a general radiative function of the surface of the black body [36], [37]. The background noise caused by the radiation of the medium can be given as [35]

$$N_{bck}(f) = \frac{2\pi hf^3}{c^2} \frac{1}{\exp\left(\frac{hf}{k_B T}\right) - 1}, \quad (20)$$

where h is the Planck constant, k_B is the Boltzmann constant, T is the temperature, and c is the speed of light in the communication medium. Note that (20) corresponds to spectral excitation of the surface of the black body [37]. For simplicity, we assume that the transmission medium is an isothermal and homogeneous medium with a thickness d . In addition, considering the absorption coefficient of the water vapor molecules, background noise p.s.d. can be formulated as [35]

$$S_{N_{bck}}(f) = \int_0^d N_{bck}(f)k(f)e^{-k(f)s} ds \quad (21)$$

$$= N_{bck}(f)(1 - e^{-k(f)d}), \quad (22)$$

where $k(f)$ is the absorption coefficient of the medium and d is the distance between the nanotransmitter and nanoreceiver. In other words, the integral in (21) describes the noise intensity at the center of a sphere with a radius d , given all the points s in the medium contribute to the noise intensity. Furthermore, by taking into account the ideal antenna aperture term, background noise can be approximated as

$$S_{N_{bck}}(f) = N_{bck}(f)(1 - e^{-k(f)d}) \frac{c^2}{4\pi f_0^2}, \quad (23)$$

where f_0 is the antenna radiation center frequency. Combining above equations, the final background noise can be given as

$$S_{N_{bck}}(f) = \lim_{d \rightarrow \infty} k_B T (1 - e^{-k(f)d}) \left(\frac{c}{\sqrt{4\pi f_0}} \right)^2. \quad (24)$$

Note that as a special case of THz communication in air, the Planck's law term in (20) is reduced to $k_B T$.

Fig. 4 shows the background noise for the THz nanocommunication considering our simulation scenario. As can be observed, the p.s.d. of the noise is very small and hence, the conventional electronic thermal noise at the receiver will play a major role. Although using the AWGN model is not ideal for the entire THz band, accurate stochastic noise models for electronic noise at THz nanoreceivers are still lacking. Therefore, in this study, we have used the AWGN model with noise power adjusted according to the E_b/N_0 values and the code length.

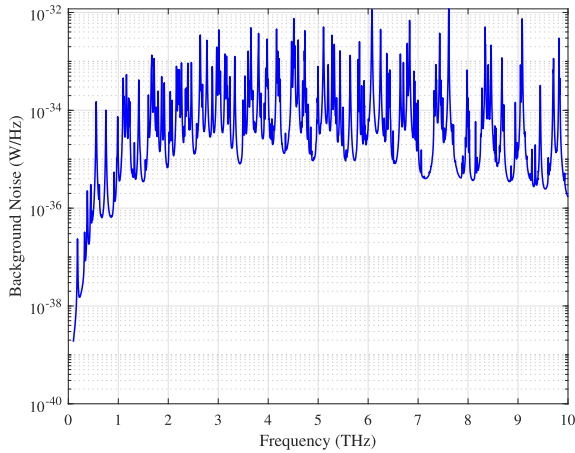


FIGURE 4. Background noise in the THz communication for the distance of $d = 0.5$ mm and $f_0 = 1.6$ THz.

Next, we assume that the nanoreceiver is exactly synchronized with the nanotransmitter. Demodulation at the nanoreceiver is performed using a noncoherent energy detection receiver. The signal is first passed through continuous-time moving average integrators, followed by a subsequent sampler. The nanoreceiver performs demodulation at the i th signal interval and produces a correlation metric of length $(L_{th} + 1)N_p$ as

$$\mathbf{r} = [\mathbf{r}_0, \dots, \mathbf{r}_{N_p-1}]^T, \quad (25)$$

with

$$\mathbf{r}_n = [r_{n,0}, \dots, r_{n,L_{th}}]^T, \quad (26)$$

where the decision variable $r_{n,j}$ is obtained as

$$r_{n,j} = \int_{iT_s+nT_f+j\delta}^{iT_s+nT_f+(j+1)\delta} r^2(t)dt, \quad (27)$$

where $r^2(t)$ is the square of the received signal [38]. Here, we observed a reduction in the computational complexity at the nanoreceiver compared to the conventional ML-PPM. In the traditional ML-PPM, the number of metrics required to process during demodulation was $(L + 1)N_p$. However, by introducing level trimming, the length of the correlation metric was significantly reduced by a factor of $(L_{th} + 1) / (L + 1)$. Therefore, based on the value of L_{th} , nanoreceiver signal processing can be significantly reduced, whereas the data rate can be significantly improved simultaneously.

Following this, based on the maximum-likelihood decision rule, we detected the position of the transmitted pulse and regenerated the multilevel signal as

$$\hat{\mathbf{m}}^{th} = [\hat{m}_1^{th}, \dots, \hat{m}_{N_p}^{th}]^T, \quad (28)$$

where

$$\hat{m}_n^{th} = \arg \max_{j=0, \dots, L_{th}} (r_{n,j}). \quad (29)$$

TABLE 2. Physical Parameters Used in the Simulations.

Parameter	Value
Pulse width (T_p)	100 fs
Level trimming threshold (L_{th})	1, 3, 5, 7
Number of multilevels (L)	5, 7
Number of pulses (N_p)	8
Distance (d)	0.5 mm
Normalizing constant (α)	$8.5 \cdot 10^{-29}$
Speed of light (c)	$2.99 \cdot 10^8$ m/s
Antenna design center frequency (f_0)	1.6 THz

Next, the demodulated multilevel signal $\hat{\mathbf{d}}$ can be described as

$$\hat{\mathbf{d}} = [\hat{d}_1, \dots, \hat{d}_{N_p}]^T, \quad (30)$$

where

$$\hat{d}_n = 2\hat{m}_n^{th} - L_{th}. \quad (31)$$

Finally, L data contained in $\hat{\mathbf{d}}$ are decoded by orthogonal codes used at the transmitter with a hard decision as

$$\mathbf{z} = \mathbf{S}^T \cdot \hat{\mathbf{d}} \quad (32)$$

and

$$\hat{\mathbf{b}} = \text{sgn}\{\mathbf{z}\}. \quad (33)$$

Owing to the level-trimming process, the demodulated multilevel signal suffers from artificial errors. However, the de-spreading process using orthogonal codes reduces the occurrence of errors owing to the processing gain [39]. Artificial errors occur owing to level trimming at the transmitter, that is, signal vector size reduction. Considering that the level trimming reduced the transmit vector size, the receiver thinks that the reduced vector size is the original transmitted vector size and starts to demodulate the signal processing the level-trimming errors. In other words, the receiver demodulates a vector, where each element of the vector possess level trimming errors. Conversely, our signal is generated by multiplication via an orthogonal code (similar to the CDMA). Considering that the signal is generated using orthogonal codes, a processing gain is achieved at the nanoreceiver. Owing to this processing gain, the performance of the proposed scheme further improves.

VI. SIMULATION RESULTS

Herein, we present the simulation environment and the results to verify the validity of the proposed scheme. For the transmission, we used a 100 fs-long Gaussian pulse with a central frequency of 1.6 THz and a 3 dB bandwidth between 0.7-2.5 THz. In other words, note that the pulse width is fixed, that is, the pulse bandwidth is fixed. Therefore, our goal is to increase the data rate within a given bandwidth, which is spectral efficiency. Additionally, the energy of the pulse was considered to be 1 aJ per energy constraint at the

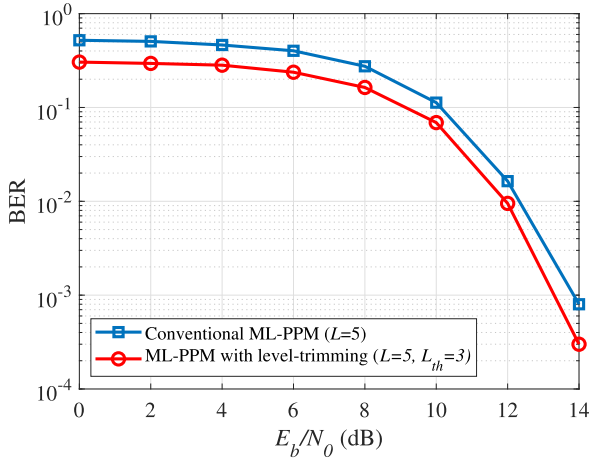


FIGURE 5. Comparison of BER performance of the enhanced ML-PPM and conventional ML-PPM schemes with $d = 0.5$ mm and $N_p = 8$.

nanolevel [30]. Walsh Hadamard codes [40] were used to generate a multilevel signal. A THz channel with a 10% water vapor concentration was considered as a transmission medium for the signal. For other atmospheric gases, their average concentrations in a dry atmosphere were used [28]. Moreover, one pulse per frame was used in the simulation. At reception, an energy detection-based nanoreceiver was considered. After extracting energy from each chip, the maximum energy was chosen as the correct position and subsequently demodulated. The number of Monte Carlo runs was fixed at 10^4 per channel. Table 2 presents the remaining simulation parameters.

As a performance metric, we decided to consider the BER and achievable data rate. The achievable data rate, R , can be defined as a function of the BER and maximum transmission data rate, R_{max} , as

$$R \triangleq R_{max}(1 - BER), \quad (34)$$

where

$$R_{max} = \frac{\text{total number of bits transmitted/symbol}}{\text{time to transmit one symbol}} \quad (35)$$

is given in bits per second (bps). Considering that $\delta = T_p$, $T_f = (L + 1)\delta$, and $T_s = N_p T_f$, the maximum achievable data rate can be expressed as

$$R_{max} = \frac{L}{N_p(L + 1)\delta}. \quad (36)$$

Similarly, the achievable data rate of the proposed ML-PPM with a level-trimming scheme is given as

$$R^{LT} = R_{max}^{LT}(1 - BER), \quad (37)$$

with

$$R_{max}^{LT} = \frac{L}{N_p(L_{th} + 1)\delta}. \quad (38)$$

Note that the BER is simulated, whereas achievable data rate, R , is numerically evaluated using (34).

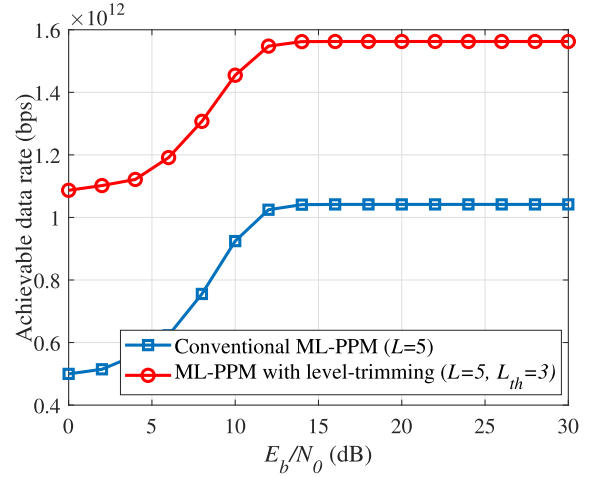


FIGURE 6. Comparison of achievable data rate performance of the enhanced ML-PPM and conventional ML-PPM schemes with $d = 0.5$ mm and $N_p = 8$.

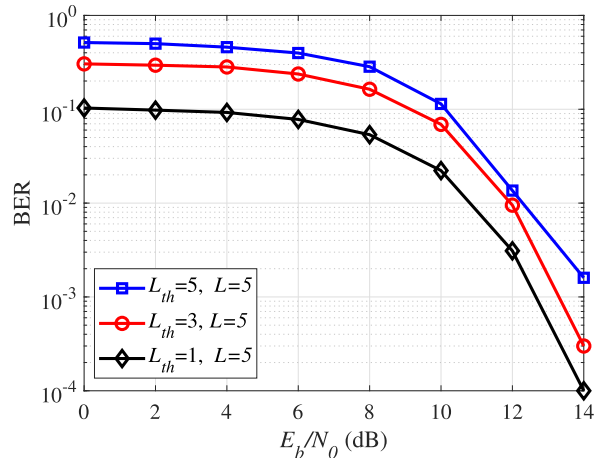


FIGURE 7. BER performance of ML-PPM with level trimming according to various threshold values of L_{th} [$d = 0.5$ mm, $N_p = 8$, and $L = 5$].

Fig. 5 compares the BER results of the proposed and conventional ML-PPM schemes for a nanocommunication distance of 0.5 mm. The value of L_{th} is 3. The figure reveals that the proposed level-trimming scheme can enhance the BER performance of the conventional scheme, considering that the allocated energy to each pulse becomes larger to maintain the same E_b/N_0 with fewer pulses. Next, Fig. 6 depicts the achievable data rate of the proposed scheme, which is extremely high compared with that of the conventional scheme. The data rate of the conventional ML-PPM saturates at approximately 1 Tbps, whereas the data rate of the proposed level-trimming scheme almost achieves a value of 1.6 Tbps. Moreover, compared to the five levels transmitted in conventional ML-PPM, level-trimming scheme eliminates two levels that has lowest occurrence probabilities and transmitted only three levels, which reduced signal processing at the nanoreceiver.

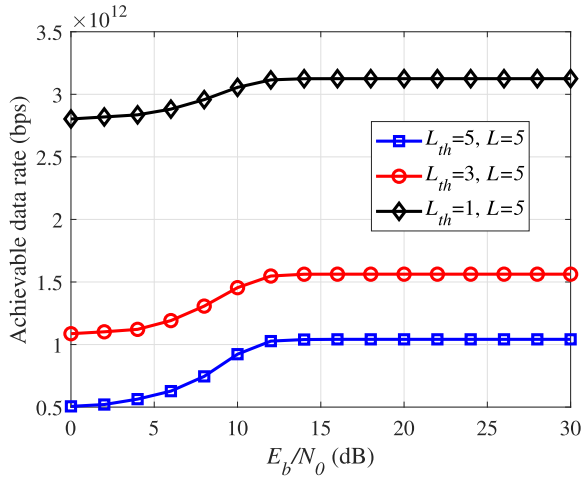


FIGURE 8. Achievable data rate performance of the enhanced ML-PPM and conventional ML-PPM schemes [$d = 0.5$ mm, $N_p = 8$, and $L = 5$].

Next, we demonstrate the effect of trimming of various levels on the ML-PPM scheme. The distance between the nanotransmitter and the nanoreceiver was fixed at 0.5 mm. Similar to the previous results, the value of L was 5. However, the values of L_{th} varied, that is, an equal number of levels were trimmed from both sides of the distribution, and only the levels with higher probabilities were transmitted (cf. Fig. 2). As presented in Fig. 7, the higher the level of trimming, the better is the BER performance. In other words, transmitting a lower number of levels with higher occurrence probabilities results in better BER performance. This can be attributed to the higher energy allocated to each pulse and the reduced correlation metric obtained via level trimming, which can minimize the possibility of error while demodulating the pulse position. For instance, in the case of $L_{th} = 1$, where we eliminated all the levels with lower probabilities and transmitted only the levels with the highest probabilities, that is, levels corresponding to -1 and 1 , we achieved the best performance. This resulted in better decoding at the nanoreceiver.

Fig. 8 presents the achievable data rate of the proposed scheme for various values of L_{th} . The data rate improved as the number of transmitted multilevels decreased. For $L_{th} = 1$, we obtained over three times the data rate compared with that in the conventional ML-PPM, that is, $L_{th} = 5$. This indicated that our proposed level-trimming scheme significantly boosted the data rate of the nanolink.

Fig. 9 illustrates the performance of the conventional ML-PPM scheme with $L = 7$. For the ML-PPM with level trimming, we used four different trimming thresholds, that is, $L_{th} = 1, 3, 5$, and 7 . The remaining parameters were maintained constant. We observed that the BER improved as L_{th} decreased. Note that as L_{th} decreased, the total number of fundamental bit energies, E_b , increased. In other words, each pulse received a larger amount of energy to maintain the same E_b/N_0 . Moreover, owing to level trimming, the number of pulse positions was reduced, which led to a denser pulse train

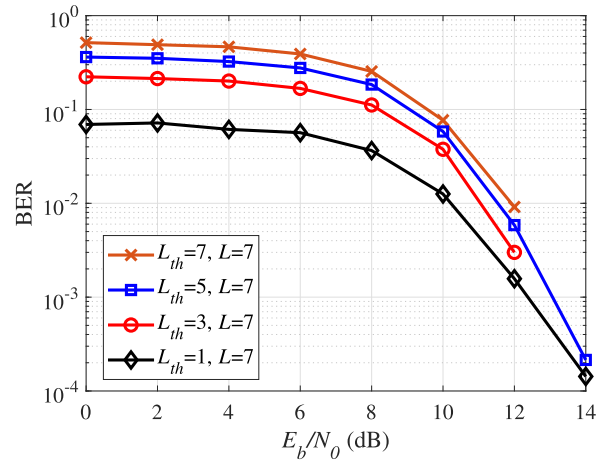


FIGURE 9. BER performance of ML-PPM with level trimming according to various threshold values of L_{th} [$d = 0.5$ mm, $N_p = 8$, and $L = 7$].

and higher average power of the signal ultimately improving the BER.

Fig. 10 presents the achievable data rate of the conventional ML-PPM scheme with $L = 7$. For the ML-PPM with level trimming, the trimming threshold values were maintained the same as above. Note that with a higher value of L , trimming threshold can also be higher. From the figure, we observed that depending on the value of trimming threshold, data rate was increased manifolds. Another interesting fact was that increasing L itself increased the data rate over one order of magnitude. For instance, with $L_{th} = 1$ and $L = 5$, we obtained a data rate of 3.125 Tbps, whereas for $L_{th} = 1$ and $L = 7$, we obtained 4.375 Tbps in the high signal-to-noise ratio region, considering that level trimming resulted in a shorter symbol duration. This results in more data transmissions per time interval. Simultaneously, it should be noted that the nanoreceiver was highly relaxed as it had to decode fewer multilevels, thereby reducing the decoding positioning errors. Overall, the proposed level-trimming approach functioned well with all trimming thresholds and improved the data rate of the conventional ML-PPM scheme. Note that the authors have not considered any numerical criteria to set the trimming threshold, and they only trimmed multilevels with lower probabilities. In other words, multilevels should always be trimmed based on the lowest occurrence probability criteria.

There is another insight that can be derived from the above simulations. From the simulation results, we found that even though level-trimming causes artificial errors, it reduces the decoding positions for the nanoreceiver, hence, improving the decoding performance. It means that reducing the number of decoding positions is much better than getting artificial errors caused by the level-trimming. In other words, even though we add artificial errors by level trimming, by reducing the number of decoding positions for the nanoreceiver, we get a better BER and achievable data rate. At the same time, computational complexity of the nanoreceiver is also reduced. Therefore, we can say that even though level trimming causes

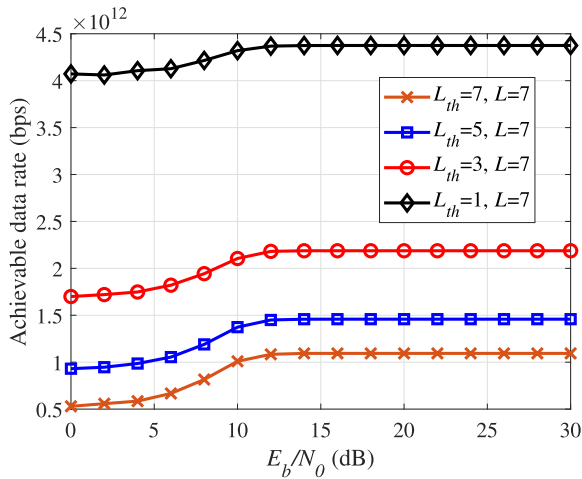


FIGURE 10. Achievable data rate performance of the enhanced ML-PPM and conventional ML-PPM schemes [$d = 0.5$ mm, $N_p = 8$, and $L = 7$].

artificial errors, it is beneficial as it improves the communication performance of the system.

VII. CONCLUSION

This paper presents a modulation scheme called ML-PPM for THz band-based nanonetworks. Furthermore, we propose an enhancement to the scheme by introducing the concept of level trimming. Level trimming significantly boosts the achievable data rate of the nanocommunication system by eliminating levels that are below a certain threshold. During our analysis, a THz channel with 10% concentration of water vapor molecules was considered. The simulation results demonstrated a maximum of approximately 2 dB gain in BER performance of the proposed level-trimming scheme compared to that of the conventional ML-PPM scheme, as well as a fourfold boost in the achievable data rate. Moreover, it addressed the complexity at the nanoreceiver, considering that it had very few levels for comparison and decoding. In addition, we can deduce that reducing the decoding position error is better than increasing the artificial errors caused by level trimming. As application domains of nanocommunications demand extremely high data rates on the order of Tbps, we believe that this study is a way forward in establishing the same.

REFERENCES

- [1] J. Wang, *Nanomachines: Fundamentals Applications*. Hoboken, NJ, USA: Wiley, 2013.
- [2] I. F. Akyildiz and J. M. Jornet, "Electromagnetic wireless nanosensor networks," *Nano Commun. Netw.*, vol. 1, no. 1, pp. 3–19, Mar. 2010.
- [3] F. Lemic, S. Abadal, W. Tavernier, P. Stroobant, D. Colle, E. Alarcon, J. Marquez-Barja, and J. Famaey, "Survey on terahertz nanocommunication and networking: A top-down perspective," *IEEE J. Sel. Areas Commun.*, vol. 39, no. 6, pp. 1506–1543, Jun. 2021.
- [4] M. H. Kabir, S. M. R. Islam, A. P. Shrestha, F. Ali, M. A. Badsha, M. J. Piran, and D.-T. Do, "Electromagnetic nanocommunication networks: Principles, applications, and challenges," *IEEE Access*, vol. 9, pp. 166147–166165, 2021.
- [5] Y. Lu, R. Ni, and Q. Zhu, "Wireless communication in nanonetworks: Current status, prospect and challenges," *IEEE Trans. Mol., Biol. Multi-Scale Commun.*, vol. 6, no. 2, pp. 71–80, Nov. 2020.
- [6] I. F. Akyildiz, J. M. Jornet, and C. Han, "TeraNets: Ultra-broadband communication networks in the terahertz band," *IEEE Wireless Commun.*, vol. 21, no. 4, pp. 130–135, Aug. 2014.
- [7] I. F. Akyildiz, J. M. Jornet, and M. Pierobon, "Nanonetworks: A new frontier in communications," *Commun. ACM*, vol. 54, no. 11, pp. 84–89, Nov. 2011.
- [8] I. F. Akyildiz, F. Brunetti, and C. Blázquez, "Nanonetworks: A new communication paradigm," *Comput. Netw.*, vol. 52, no. 12, pp. 2260–2279, Aug. 2008.
- [9] Q. H. Abbasi, K. Yang, N. Chopra, J. M. Jornet, N. A. Abuali, K. A. Qaraqe, and A. Alomainy, "Nano-communication for biomedical applications: A review on the state-of-the-art from physical layers to novel networking concepts," *IEEE Access*, vol. 4, pp. 3920–3935, 2016.
- [10] X.-X. Yin, A. Baghai-Wadji, and Y. Zhang, "A biomedical perspective in terahertz nano-communications—A review," *IEEE Sensors J.*, vol. 22, no. 10, pp. 9215–9227, May 2022.
- [11] I. F. Akyildiz, J. M. Jornet, and C. Han, "Terahertz band: Next frontier for wireless communications," *Phys. Commun.*, vol. 12, pp. 16–32, Sep. 2014.
- [12] I. F. Akyildiz, A. Kak, and S. Nie, "6G and beyond: The future of wireless communications systems," *IEEE Access*, vol. 8, pp. 133995–134030, 2020.
- [13] T. S. Rappaport, Y. Xing, O. Kanhere, S. Ju, A. Madanayake, S. Mandal, A. Alkhatieb, and G. C. Trichopoulos, "Wireless communications and applications above 100 GHz: Opportunities and challenges for 6G and beyond," *IEEE Access*, vol. 7, pp. 78729–78757, 2019.
- [14] I. F. Akyildiz and J. M. Jornet, "The internet of nano-things," *IEEE Wireless Commun.*, vol. 17, no. 6, pp. 58–63, Dec. 2010.
- [15] M. Miraz, M. Ali, P. Excell, and R. Picking, "Internet of nano-things, things and everything: Future growth trends," *Future Internet*, vol. 10, no. 8, p. 68, Jul. 2018.
- [16] J. M. Jornet and I. F. Akyildiz, "The internet of multimedia nano-things," *Nano Commun. Netw.*, vol. 3, no. 4, pp. 242–251, 2012.
- [17] I. F. Akyildiz, C. Han, Z. Hu, S. Nie, and J. M. Jornet, "Terahertz band communication: An old problem revisited and research directions for the next decade," *IEEE Trans. Commun.*, vol. 70, no. 6, pp. 4250–4285, Jun. 2022.
- [18] K. D. Paschaloudis, C. L. Zekios, G. C. Trichopoulos, F. Farmakis, and G. A. Kyriacou, "An eigenmode study of nanoantennas from terahertz to optical frequencies," *Electronics*, vol. 10, no. 22, p. 2782, Nov. 2021.
- [19] H. Elayan, O. Amin, B. Shihada, R. M. Shubair, and M.-S. Alouini, "Terahertz band: The last piece of RF spectrum puzzle for communication systems," *IEEE Open J. Commun. Soc.*, vol. 1, pp. 1–32, 2020.
- [20] Z. Xiao, Q. Yang, J. Huang, Z. Huang, W. Zhou, Y. Gao, R. Shu, and Z. He, "Terahertz communication windows and their point-to-point transmission verification," *Appl. Opt.*, vol. 57, no. 27, pp. 7673–7680, Sep. 2018.
- [21] M. Nafari and J. M. Jornet, "Modeling and performance analysis of metallic plasmonic nano-antennas for wireless optical communication in nanonetworks," *IEEE Access*, vol. 5, pp. 6389–6398, 2017.
- [22] J. M. Jornet and I. F. Akyildiz, "Graphene-based plasmonic nano-transceiver for terahertz band communication," in *Proc. 8th Eur. Conf. Antennas Propag. (EuCAP)*, Apr. 2014, pp. 492–496.
- [23] J. M. Jornet and I. F. Akyildiz, "Graphene-based plasmonic nano-antenna for terahertz band communication in nanonetworks," *IEEE J. Sel. Areas Commun.*, vol. 31, no. 12, pp. 685–694, Dec. 2013.
- [24] I. F. Akyildiz, C. Han, Z. Hu, S. Nie, and J. M. Jornet, "Terahertz band communication: An old problem revisited and research directions for the next decade," *IEEE Trans. Commun.*, vol. 70, no. 6, pp. 4250–4285, Jun. 2022.
- [25] K. Tekbıyık, A. R. Ekti, G. K. Kurt, and A. Görçin, "Terahertz band communication systems: Challenges, novelties and standardization efforts," *Phys. Commun.*, vol. 35, Aug. 2019, Art. no. 100700.
- [26] M. J. Marcus, "Progress in opening access to spectrum above 100 GHz," *IEEE Wireless Commun.*, vol. 26, no. 2, pp. 2–3, Apr. 2019.
- [27] I. F. Akyildiz, M. Pierobon, S. Balasubramaniam, and Y. Koucheryavy, "The internet of bio-nano things," *IEEE Commun. Mag.*, vol. 53, no. 3, pp. 32–40, Mar. 2015.

- [28] J. M. Jornet and I. F. Akyildiz, "Channel modeling and capacity analysis for electromagnetic wireless nanonetworks in the terahertz band," *IEEE Trans. Wireless Commun.*, vol. 10, no. 10, pp. 3211–3221, Oct. 2011.
- [29] E. Zarepour, M. Hassan, C. T. Chou, and S. Bayat, "Performance analysis of carrier-less modulation schemes for wireless nanosensor networks," in *Proc. IEEE 15th Int. Conf. Nanotechnol. (IEEE-NANO)*, Jul. 2015, pp. 45–50.
- [30] J. M. Jornet and I. F. Akyildiz, "Femtosecond-long pulse-based modulation for terahertz band communication in nanonetworks," *IEEE Trans. Commun.*, vol. 62, no. 5, pp. 1742–1754, May 2014.
- [31] P. Singh, B.-W. Kim, and S.-Y. Jung, "TH-PPM with non-coherent detection for multiple access in electromagnetic wireless nanocommunications," *Nano Commun. Netw.*, vol. 17, pp. 1–13, Jan. 2018.
- [32] P. Singh and S.-Y. Jung, "Performance analysis of time-hopping multiple access using multi-level PPM for terahertz nanocommunication," TechRxiv, Dec. 2022, doi: [10.36227/techrxiv.20265885.v1](https://doi.org/10.36227/techrxiv.20265885.v1).
- [33] A. Papoulis and S. U. Pillai, *Probability, Random Variables, and Stochastic Processes*, 4th ed. New York, NY, USA: McGraw-Hill, 2002.
- [34] P. Sen and J. M. Jornet, "Experimental demonstration of ultra-broadband wireless communications at true terahertz frequencies," in *Proc. IEEE 20th Int. Workshop Signal Process. Adv. Wireless Commun. (SPAWC)*, Jul. 2019, pp. 1–5.
- [35] J. Kokkonen, J. Lehtomäki, and M. Juntti, "A discussion on molecular absorption noise in the terahertz band," *Nano Commun. Netw.*, vol. 8, pp. 35–45, Jun. 2016.
- [36] R. Zhang, K. Yang, Q. H. Abbasi, K. A. Qaraqe, and A. Alomainy, "Analytical modelling of the effect of noise on the terahertz *in-vivo* communication channel for body-centric nano-networks," *Nano Commun. Netw.*, vol. 15, pp. 59–68, Mar. 2018.
- [37] S. Chandrasekhar, *Radiative Transfer*. Chelmsford, MA, USA: Courier Corporation, 2013.
- [38] R. G. Cid-Fuentes, J. M. Jornet, I. F. Akyildiz, and E. Alarcón, "A receiver architecture for pulse-based electromagnetic nanonetworks in the terahertz band," in *Proc. IEEE Int. Conf. Commun. (ICC)*, Jun. 2012, pp. 4937–4942.
- [39] R. A. Scholtz, "The spread spectrum concept," *IEEE Trans. Commun.*, vol. COM-25, no. 8, pp. 748–755, Aug. 1977.
- [40] K. J. Horadam, *Hadamard Matrices and Their Applications*. Princeton, NJ, USA: Princeton Univ. Press, 2012, doi: [10.1515/9781400842902](https://doi.org/10.1515/9781400842902).



PANKAJ SINGH (Member, IEEE) received the B.E. degree in electronics and communication engineering from Gujarat University, Ahmedabad, Gujarat, India, in 2009, and the combined M.S.-Ph.D. degree in electronic engineering from Yeungnam University, Gyeongsang, Gyeongsangbuk, South Korea, in 2019.

From March 2019 to August 2019, he served as a Postdoctoral Researcher at the Ubiquitous Communications Laboratory. He is currently an Assistant Professor at the Department of Electronic Engineering, Yeungnam University. His research interests include electromagnetic nanonetworks, molecular communications, and optical camera communications.

Prof. Singh is a member of the Institute of Electronics and Information Engineers (IEIE). He was a recipient of the Outstanding Graduate Student Award in the Daegu and Gyeongbuk Province awarded by the IEIE, South Korea, in 2018.



SUNG-YOON JUNG (Member, IEEE) received the B.S. degree in electrical engineering from Korea University, Seoul, South Korea, in 2000, and the M.S. and Ph.D. degrees in electrical engineering from the Korea Advanced Institute of Science and Technology (KAIST), in 2002 and 2006, respectively.

From 2006 to 2009, he worked as a Senior Engineer with the Telecommunication Research and Development Center, Samsung Electronics Co., Ltd. Since 2009, he has been associated with Yeungnam University, where he is currently a Professor with the Department of Electronic Engineering. He has also been a Visiting Professor with the Department of Electrical and Computer Engineering and the Department of Epidemiology, University of Florida, Gainesville, FL, USA, in 2015 and 2019, respectively. His research interests include signal processing for wireless communications, optical wireless communications, electromagnetic nanocommunications, molecular communications, 5G and 6G communications, and machine learning.

• • •